

Technical Report

TR-24-06

December 2024



Evaluation of microstructural defects in wedge-open loaded stress corrosion cracking specimens from the MiniCan field test

James Hesketh

Johannes Johansson

SVENSK KÄRNBRÄNSLEHANTERING AB

SWEDISH NUCLEAR FUEL
AND WASTE MANAGEMENT CO

Box 3091, SE-169 03 Solna
Phone +46 8 459 84 00
skb.se

SVENSK KÄRNBRÄNSLEHANTERING

ISSN 1404-0344

SKB TR-24-06

ID 2063660

December 2024

Evaluation of microstructural defects in wedge-open loaded stress corrosion cracking specimens from the MiniCan field test

James Hesketh, Amentum Clean Energy Limited

Johannes Johansson, Svensk Kärnbränslehantering AB

This report is published on www.skb.se

© 2024 Svensk Kärnbränslehantering AB

Executive Summary

In the MiniCan 3 and 4 field tests, fatigue pre-cracked WOL specimens were exposed to the ca 1 μM sulfidic Äspö groundwater for up to 9 years whilst in the unloaded state. Metallographic examination of these specimens showed signs of general corrosion but also revealed small (up to 100 μm) secondary fractures emanating from the WOL fatigue pre-cracked area. Since SCC is not expected to occur in copper under the MiniCan test conditions, i.e. anoxic with sulfide concentrations in the μM range, another explanation was sought. A plausible explanation of the secondary fractures could be that these are induced in the material during fatigue pre-cracking. In order to evaluate the fatigue hypothesis, two new WOL specimens, BBG01 and BBG02, were manufactured and fatigue pre-cracked. This was done using similar procedures as those used in manufacturing of the MiniCan WOL specimens.

Metallographic examination of cross-sections of the new (BBG01 and BBG02) WOL specimens was performed using SEM, leading to the following conclusions:

Fatigue pre-cracking of new WOL specimens produced cracks that closely resembled those observed previously on unloaded, pre-cracked WOL specimens following exposure to sulphidic groundwater in a borehole for between 4 and 9 years during the MiniCan experiment.

Cracks that were produced by fatigue only (i.e., with no exposure to the borehole environment) exhibited secondary cracks branching from the main pre-crack, with some secondary cracks orientated perpendicular to it. Similar to the specimens from the MiniCan experiment, multiple crack initiation was observed from the notch of the new WOL specimens.

The presence of secondary cracks and multiple crack initiation from the notch that was observed on WOL specimens taken from the MiniCan experiment is most likely attributed to the initial fatigue pre-cracking and are thus not signs of stress corrosion cracking during exposure to Äspö groundwater. This is due to the close resemblance that these crack features share with those of the new WOL specimens were produced by fatigue only (i.e., with no exposure to the borehole environment).

The formation of secondary fractures during fatigue loading was further evidenced by the presence of cracks that emanated perpendicular to the fracture face of the fast fracture region that was formed when fatigue cycling was applied post-test to open the WOL specimens from MiniCan 3 for inspection of the corroded surface.

Contents

1	Introduction	7
1.1	Background	7
1.2	WOL specimens from MiniCan 3	8
1.3	WOL specimens from MiniCan 4	10
1.4	Hypotheses	11
2	Materials and Methods	13
2.1	Manufacture of new copper WOL specimens	13
2.2	Metallographic preparation and examination	13
3	Results	15
4	Discussion	17
5	Conclusions	23
	References	25
Appendix A	Location of U-bend and WOL specimens in MiniCan borehole	27
Appendix B	Manufacturing of the original MiniCan WOL specimens	29
Appendix C	Preparation of new WOL specimens	31

1 Introduction

1.1 Background

A series of five in situ corrosion experiments, known as the MiniCan experiments, have been operating in the Äspö Hardrock Laboratory since 2007 (Smart and Rance, 2009). The experiments made use of small-scale model canisters (MiniCan) that incorporated the main features of the KBS-3 canister design (i.e. a copper shell around a cast iron insert). The original aim of the experiments was to evaluate how a small defect in the copper shell could affect the corrosion of the cast iron insert, and in turn how the iron corrosion process could affect the canister geometry and integrity over time. Five experimental packages (referred to as MiniCan 1 to 5), comprising miniature canisters, were installed in individual near-horizontal boreholes at ca 420 m depth and the boreholes were sealed in order to maintain anoxic conditions.

The five packages differed regarding the number and position of defects through the copper shell, as well as in the emplacement configuration within the borehole. Three of the five canisters (MiniCan 1 to 3) were housed within a support cage containing bentonite that conditioned the groundwater prior to reaching the canister whilst preventing direct contact between the canister surface and bentonite. The fourth canister (MiniCan 4) was emplaced directly in bentonite to simulate repository exposure conditions more closely. The fifth canister (MiniCan 5) was emplaced with no bentonite to examine the potential influence of the formation of a biofilm. In addition to the miniature canisters, instrumentation including electrodes, corrosion coupons, and stress corrosion cracking (SCC) specimens were also installed in each borehole (see Appendix A). Further details regarding the setup of the MiniCan test series can be found in Smart and Rance (2009), and details regarding the continuous monitoring of electrochemical parameters and results from measurements of groundwater chemistry can be found in Smart et al. (2015). The results of the retrieval and post-test examination of MiniCan 3 are reported in Smart et al. (2012), while the results for MiniCan 4 and 5 are found in Gordon et al. (2017).

Two types of specimens were installed in MiniCan 3 and 4 to evaluate the susceptibility of copper to SCC during exposure to corrosive groundwater: i) U-bend specimens and ii) wedge-open loaded (WOL) specimens. The U-bend specimens were used to evaluate the susceptibility of copper to crack initiation whilst subjected to tensile stress and a high degree of deformation. The wedge-open loaded specimens were used to evaluate the susceptibility of copper to crack growth. WOL specimens were pre-cracked in air using a high frequency fatigue machine to achieve a crack with a nominal length of 1.5 mm. The location and direction of the pre-crack in WOL specimens is shown in Figures 1-6 and B-2. No additional loading was applied to the WOL specimens (Smart et al. 2013), meaning that only residual stresses due to machining, grinding and polishing, may have remained after sample preparation and fatigue cracking were present. The U-bend and WOL specimens were installed in the boreholes without any contact with the bentonite clay, i.e. they were directly exposed to the groundwater. Given the absence of bentonite in the experimental setup the conditions in the borehole are expected to have been advective.

This report concerns the post-test examination of WOL specimens from MiniCan 3 and 4, following exposure to the borehole environment for 4 and 9 years, respectively. New WOL specimens were also manufactured and examined in order to better understand the observations made in the MiniCan specimens. Detailed descriptions and photographs of the WOL specimens can be found in the references given above and are also given in Appendices B and C in this report.

The aim of this work was to evaluate whether the cracking that was observed on the WOL samples taken from the MiniCan experiment could have been produced entirely through dynamic mechanical loading i.e., fatigue as opposed to SCC.

1.2 WOL specimens from MiniCan 3

The specimens installed in MiniCan 3 were examined visually after the retrieval in 2011 (Smart et al. 2012) and were later examined further by metallographic methods (Smart et al. 2013), (Aggarwal et al. 2015). Metallographic examination using Scanning Electron Microscopy (SEM) of the WOL specimens from MiniCan 3 showed branching from the pre-crack, with cracks of the order of 10 to 100 μm in size emanating from the pre-crack, see e.g. Figure 1-1 and Figure 1-2 reproduced from (Smart et al. 2013).

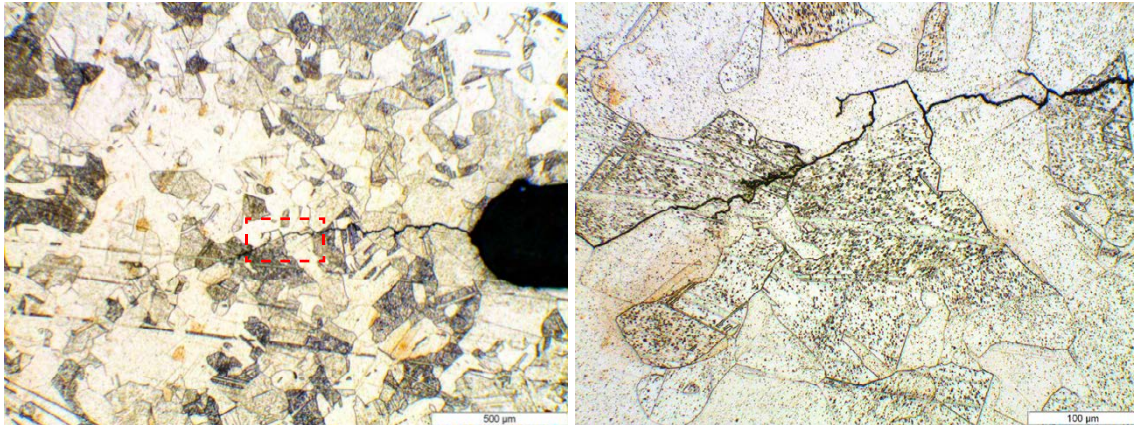


Figure 1-1. Optical micrograph of cross-section through WOL specimen 1 (near borehole flange – shown in Appendix A) from MiniCan 3 (Figure 3-16 in Smart et al. (2013)) showing entire crack length (left) and zoomed section (right). The specimen was etched in NH_4OH (S.G. 88) + H_2O + H_2O_2 (equal volumes) for 20 seconds to show grain boundaries.

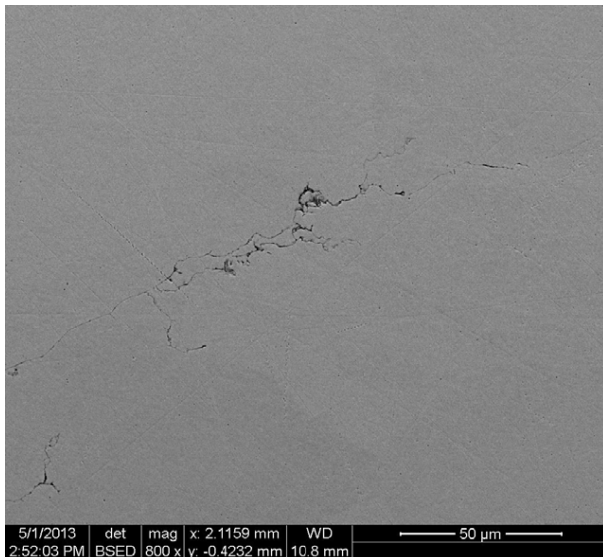


Figure 1-2. SEM micrograph of cross-section through WOL specimen 1 (near borehole flange – shown in Appendix A) from MiniCan 3 (from Figure 3-20 in Smart et al. (2013)) showing crack branching.

During further metallographic examination, the two WOL specimens from MiniCan 3 were broken apart by fatigue crack opening (fast fracture) to expose the fracture surfaces for analysis. The original pre-cracked surface was easily distinguished from the new fractured area (created post-test) since the latter exhibited a shiny metallic face, while the original pre-cracked surface was covered by a dark deposit (e.g. Figure 1-3 taken from (Aggarwal et al. (2015))). Energy Dispersive X-ray Spectroscopy (EDS) of the dark deposit was consistent with it being a copper oxide. Although the nominal target length of the pre-crack was 1.5 mm, the lengths of the pre-crack measured after opening the specimens varied within 935–1258 μm and 1631–1961 μm for the two WOL specimens, respectively. Accounting for the uncertainty in the crack length associated with the pre-cracking procedure, which was several hundred microns, there were no obvious signs of growth of the pre-crack in these specimens during exposure (Aggarwal et al. 2015). Examination of the fracture surfaces by SEM using secondary electron imaging showed smaller secondary fractures of the order of ca 100 μm , which appeared to emanate from the shiny fast fracture surface and extend inwards (i.e. perpendicular to the main fracture surface). The location of these fractures implies that they were formed during fatigue fracturing that was performed to open the specimen for examination after exposure in the borehole, see e.g. fast fracture area in Figure 1-3 and Figure 1-4, reproduced from (Aggarwal et al. 2015).

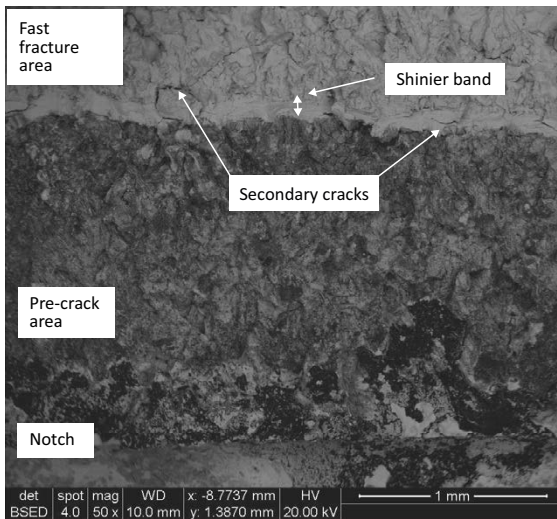


Figure 1-3. SEM image of WOL specimen B1 (near to borehole flange – shown in Appendix A) from MiniCan 3, end of pre-crack, $\times 50$ magnification (from Figure 3-10 in Aggarwal et al. (2015)).

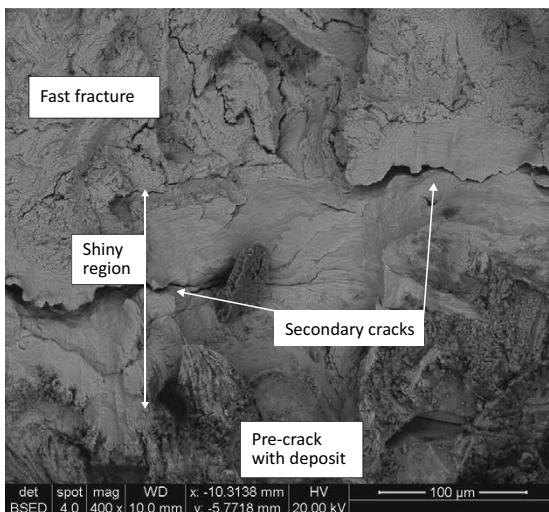


Figure 1-4. SEM image of WOL specimen B2 (near to borehole flange – shown in Appendix A) from MiniCan 3, end of pre-crack, $\times 400$ magnification (from Figure 3-12 in Aggarwal et al. (2015)). Note the ca 100 μm fractures in the fast fracture surface.

1.3 WOL specimens from MiniCan 4

MiniCan 4 was retrieved in 2015 (Gordon et al. 2017). The surfaces perpendicular to the crack generated through fatigue loading (pre-cracked specimens) were polished and examined with Light Optical Microscopy (LOM), while SEM was used to determine the crack length. One of the specimens was opened to expose the fracture surfaces by fast fracture, as described previously. SEM-EDS analysis of the WOL samples detected the presence of small amounts of sulfur at the crack tip in the surface oxide. As with the MiniCan 3 specimens, secondary fractures (up to ca 100 μm) were noted seemingly emanating from the main pre-crack into the cold deformation area of the parent material on either side of it, see e.g., Figure 1-5. Some of the secondary fractures that branched from the main pre-crack were orientated perpendicular to the direction of the pre-crack, i.e. parallel to the direction of the applied load during fatigue pre-cracking and exhibited subsequent branching. Furthermore, a secondary crack ca 100 μm in length was observed emanating from the notch ca 150 μm from the opening of the main pre-crack, see Figure 1-6.

It was noted in Gordon et al. (2017) that the branching cracks that emanated from the main pre-crack were not consistent with SCC as they were mainly transgranular, which is more typically associated with fatigue. The formation of branching cracks during fatigue is consistent with the observation of secondary fracture surfaces perpendicular to the main pre-crack in the fast fracture surface of a WOL specimen from MiniCan 3 (see Figure 1-3 and Figure 1-4), which imply that post-test fatigue used to open the fracture surfaces also leads to secondary cracking. In addition, an EDS line-scan across a small branching fracture in one of the WOL specimens from MiniCan 4 showed the presence of oxygen and silicon only. The absence of either sulphur or chlorine in the fracture suggests that it was formed by fatigue rather than SCC (see Figure A3-39 in Gordon et al. (2017)).

Analysis of the fracture surface of one of the two WOL specimens from MiniCan 4 showed that the fracture surface of the exposed pre-crack could easily be distinguished from the new fracture surface due to differences in their visual appearances (e.g. Figure 1-3, taken from Gordon et al. (2017)). EDS analysis of the pre-crack surface showed mainly oxygen and silicon, and up to a few at. % sulfur. The length of the original pre-crack was estimated to 1.59 mm on one side and 1.75 mm on the other, which is in reasonable agreement with the nominal target value for the pre-crack (1.5 mm), when considering the uncertainty associated with the pre-cracking process.



Figure 1-5. Optical image of the middle part of the pre-crack of WOL sample M4 4:1 from MiniCan 4, showing smaller fractures emanating from the pre-crack (Figure 4-7 in Gordon et al. (2017)).

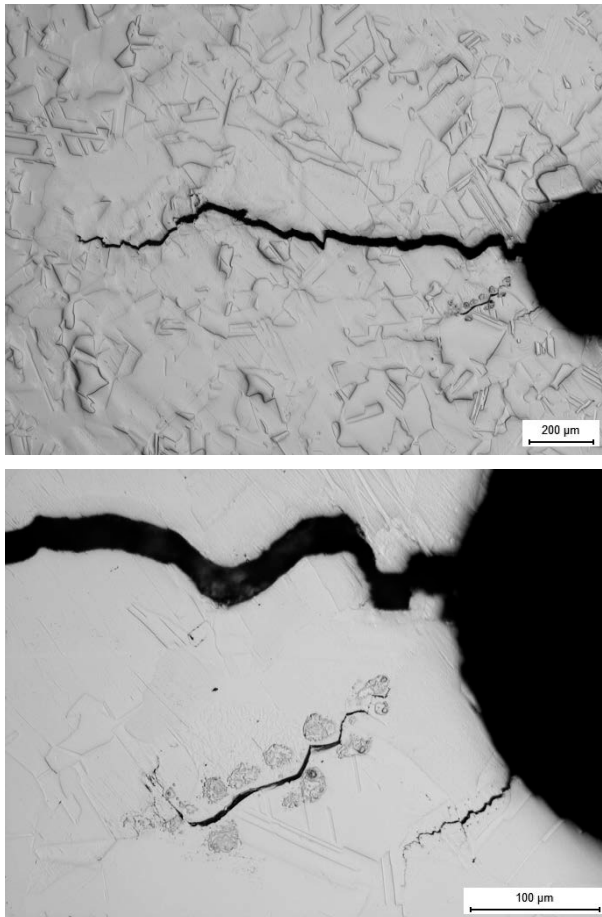


Figure 1-6. Optical micrographs of the same region of WOL specimen at a coarser (top) and finer (bottom) scale showing small secondary fractures close to and emanating from the notch of WOL specimen (M4 3:1) from MiniCan 4, the cracks are below the main fatigue pre-crack (Figure A3-35 in Gordon et al. (2017)).

1.4 Hypotheses

Two hypotheses exist to explain the presence of secondary cracks branching from the main fatigue crack. The first hypothesis is that the secondary cracks formed due to fatigue during pre-cracking and is referred to as the *fatigue hypothesis*. The second hypothesis is that the secondary cracks formed due to SCC whilst being exposed to the groundwater in the borehole and is referred to as the *SCC hypothesis*, which was the interpretation proposed in an external expert review commissioned by the Swedish regulator (SSM, 2019). This work presents no new chemical data for further evaluation of the SCC hypothesis.

In this work, the fatigue hypothesis has been evaluated further by preparing new fatigue-cracked WOL specimens for direct metallographic examination without exposure to the borehole environment. It was reasoned that if the new specimens exhibited fracture branching of the same type and size as was observed in the specimens from MiniCan 3 and 4, this would support the hypothesis that the cracks observed on the MiniCan specimens formed due to fatigue and not SCC.

2 Materials and Methods

2.1 Manufacture of new copper WOL specimens

New WOL specimens were manufactured as per the specifications of the original MiniCan specimens based on the methodology reported in (Smart et al. 2013), original drawings, and previous records of the procedure (Appendix B). Additional efforts were made to reproduce the original manufacturing procedure as closely as possible, e.g. undertaking the manufacture and fatigue pre-cracking in the same laboratory as the original samples using identical equipment.

The material used to manufacture the new WOL specimens was oxygen-free phosphorus-doped copper (OFP-Cu) provided by SKB and taken from the copper tube denoted T66 at SKB's canister laboratory in Oskarshamn. Using the information in Appendix B, a slice of material was removed at the Amentum Harwell Laboratory using a bandsaw, followed by the extraction of two specimens by Electrical Discharge Machining (EDM). Finally, a drill tap was used to add the thread to the specimens. The original WOL specimens in MiniCan were machined from a scrap copper lid provided by SKB (Smart and Rance, 2009). The new specimens underwent fatigue pre-cracking using a Si-Plan high frequency fatigue machine (Vibrophore), believed to have been used also for the original specimens, calibrated to ISO 7500-1:2018. New shackles had to be manufactured, using original drawings, as the original shackles were not available. Due to complications with overload and plastic deformation of the specimens during pre-cracking, several specimens had to be manufactured from the original slice. Details of the fault investigation are described in Appendix C. When a stable procedure had been established, the successfully manufactured pre-cracked WOL specimens were given the internal specimen IDs BBG01 and BBG02.

Fatigue pre-cracking was performed to produce a crack of ca 1.5 mm in length, leading to a crack length-to-width ratio of $a/W \approx 0.4$. The stress intensity factor used was $K_{\max} = 8.5 \text{ MPa } \sqrt{\text{m}}$ with an R-ratio of 0.1, and the frequency was ca 100 Hz.

2.2 Metallographic preparation and examination

Following manufacture and fatigue pre-cracking, specimens BBG01 and BBG02 were cross-sectioned through the centreline of the thickness. The sections were then mounted in a conductive resin, ground and finally polished to a 0.25 μm finish. The metallographically prepared specimens were examined by SEM. After the initial SEM examination, the WOL specimens were then etched in a solution comprising 5 % NH_4OH , 25 ml deionised water and 25 to 50 ml H_2O_2 . After etching, they were once again examined in the SEM.

3 Results

Figure 3-1 and Figure 3-2 show pre- and post-etching SEM images of the newly manufactured WOL specimens BBG01 and BBG02, respectively. In both instances, the team who produced the cracks inspected them and deemed them to be typical of those produced during pre-cracking. Some features appeared more clearly after etching, but etching did not seem to cause any other changes in the morphology of the pre-crack. Both specimens exhibited clear evidence of secondary branching cracks, emanating from the main pre-crack as well as from the notch.



Figure 3-1. SEM micrographs of the WOL specimen BBG01 pre-etch (left) and post-etch (right) that was pre-cracked by fatigue but was not exposed to a corrosive environment prior to metallographic analysis. Some features appear more clearly after etching the specimen surface.

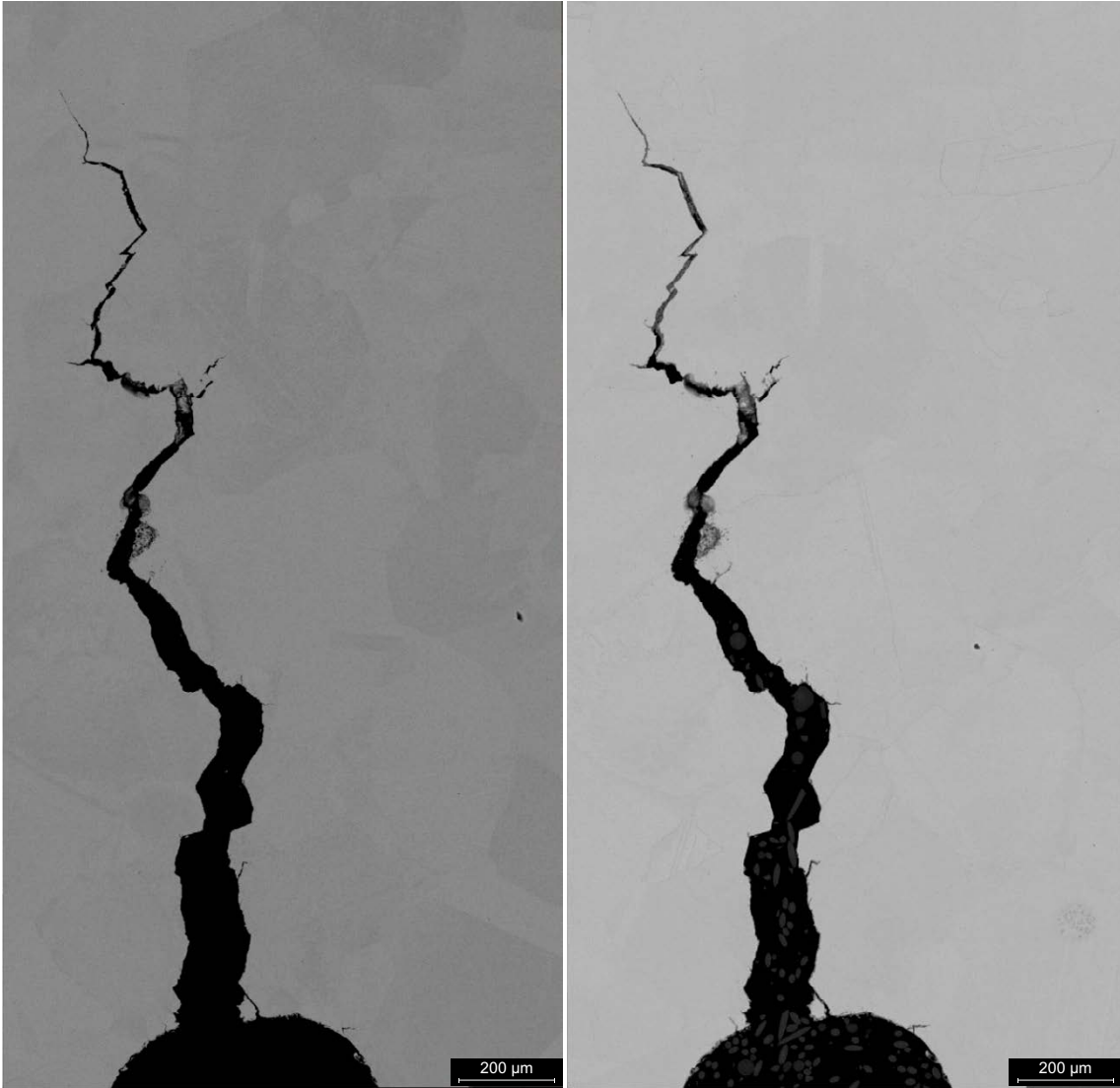


Figure 3-2. SEM micrographs of WOL specimen of BGG02 pre-etch (left) and post-etch (right) that was pre-cracked by fatigue but was not exposed to a corrosive environment prior to metallographic analysis.

4 Discussion

In Gordon et al. (2017) it was noted that the appearance of the secondary fractures observed in WOL specimens from MiniCan 3 and 4 were not consistent with SCC. However, this was not the conclusion of an external expert review ordered by the Swedish regulator (SSM, 2019), which stated that the cracks were typical of SCC and possibly attributed them to hydrogen charging. The evidence in favor of the SCC hypothesis rests on the observation that the secondary cracks are branched and extend away from the main pre-crack in different orientations and a reported hydrogen content in the outer wall of the MiniCan 5 of up to 1.8 wt-ppm (SSM, 2019). The SCC hypothesis also requires the presence of significant residual tensile stresses within the WOL specimens, which have neither been confirmed nor dismissed.

The sulphide concentration in the MiniCan borehole was measured several times during the experiment and was consistently found to be approximately 1 μM . The chloride concentration was measured across the five experiments and varied between roughly 0.2 to 0.3 M between 2008 and 2010 (Smart et al. 2015). Superficial cracking of copper in anoxic sulphide solutions has been reported for sulphide concentrations of 1 mM or higher during slow-strain testing, while no signs of cracking were observed at a lower sulphide concentration of 20 μM with 10 mM chloride (Taxén et al. 2023). In addition, the superficial cracking of 10 to 20 μm that was observed in experiments with high sulphide concentrations had the appearance of intergranular corrosion (IGC) rather than SCC (Taxén et al. 2023). Similarly, intergranular cracking of OFP-copper has been reported to occur at sulphide concentrations of 1 mM in the presence of 100 mM chloride when evaluated by slow strain rate testing (SSRT) at 90 °C but did not occur at a lower sulphide concentration of 10 μM (Forsström et al. 2021). Furthermore, SSRT of pure copper (with 45 ppm phosphorous) at 80 °C in synthetic seawater, which has a comparatively high chloride concentration of 0.56 M, identified the sulphide threshold for SCC to be in the range of 5 to 10 mM (Taniguchi and Kawaski 2008). Cracking is thus not expected under the conditions of the MiniCan tests as the measured sulphide concentration in the groundwater is considerably lower than the threshold concentration found in other studies.

The secondary cracks observed on the WOL specimens from the MiniCan experiment were reported as being transgranular (Gordon et al. 2017), which differs from those reported by Forsström et al. (2021), Taxén et al. (2023) and Taniguchi and Kawaski (2008) who reported intergranular cracking. A key difference between the laboratory tests and the conditions that the WOL specimens were exposed to is the temperature. The WOL specimens were exposed to the borehole which had an ambient temperature of 15 °C (Smart et al. 2015), whereas the laboratory tests were performed at elevated temperatures. High temperature typically exacerbates localised corrosion and SCC, notwithstanding the exception of the susceptibility to SCC that copper exhibits in nitrates that is reported to decrease at increasing temperature (Ikeda and Litke, 2007). Furthermore, the laboratory tests were performed under dynamic tensile loading whereas the WOL specimens were likely unloaded. In Smart et al. 2013, it was concluded based on findings during retrieval and post-test examination that the WOL specimens were not subjected to an applied load before being installed. Thus, the only stresses that could have driven SCC in the WOL specimens are residual stresses.

The fatigue hypothesis is supported by several observations, the main one being the similarity between the crack features on the WOL specimens retrieved from the MiniCan experiment and the newly prepared WOL specimens examined directly after preparation. The following similarities are noted:

- The pre-cracks in the new WOL specimens are nominally of the same length (1.5 ± 0.3 mm) as the pre-cracks of the MiniCan specimens and the fracture morphology appeared similar. Comparing Figure 3-1 and Figure 3-2 with Figure 4-1 and Figure 4-2 show that in both cases the cracks are mainly transgranular. However, Gordon et al. (2017) reported the pre-crack to be mostly intergranular, and Figure 1-1 appears to show the pre-crack as both transgranular and intergranular.
- For both the new specimens and the MiniCan specimens there are small secondary fractures emanating from the main pre-crack.
- For both the new specimens and the MiniCan specimens, the number and length of the secondary fractures are similar. Comparing Figure 3-1 and Figure 3-2 with Figure 4-1 to Figure 4-4 there are 3 to 7 secondary fractures per ca 1.5 mm (primary) pre-crack, and the secondary fractures vary

in length from a few tens of μm up to ca 100 μm . (It is acknowledged that further inspection of the specimens using high resolution may enable detection of a greater number of small cracks per unit length).

- In both the new specimens and the MiniCan specimens there are secondary fractures extending around one or several crystal grains, which then appear to be “detached” when viewed in cross-section (two dimensional). These seem to occur in the cold deformed zone near the surface. Examples can be seen e.g. in Figure 3-2 close to the opening of the pre-crack at the notch, near the corresponding position in Figure 4-4, and in close-up in Figure 4-5.
- In both the new specimens and in the MiniCan specimen there are fractures of up to ca 100 μm length, extending from the notch near the opening of the pre-crack. This can be seen for both the new specimens in Figure 3-1 and Figure 3-2, as well as for the MiniCan specimens in Figure 1-6 and Figure 4-6.

The fatigue hypothesis is further supported by the observation of fractures of similar size (ca 100 μm) in the fast fracture surface of WOL specimens from MiniCan 3 (Figures 1-3 and 1-4), after further fatigue cracking was used to open up the specimens for SEM-EDS analysis of the fracture surface, as reported in Aggarwal et al. (2015).

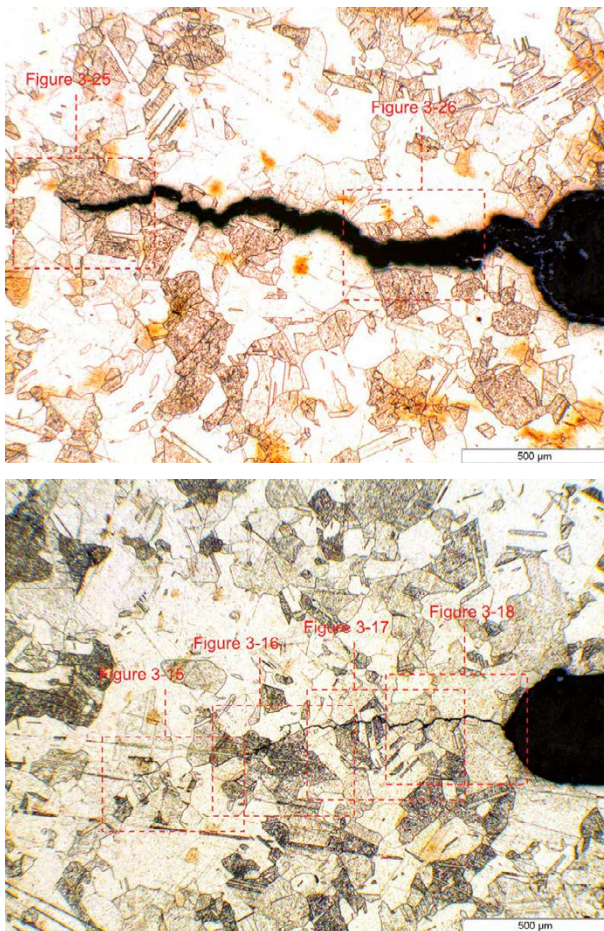


Figure 4-1. Optical micrographs of the pre-cracks in WOL specimen 2 (top) and WOL specimen 1 (bottom) from MiniCan 3 (Figures 3-14 and 3-24 in (Smart et al. 2013)). Figure numbers in the images refer to figures in the report (Smart et al. 2013).

Crack branching of ultrafine-grained copper during fatigue testing has been reported in literature previously (Collini, 2012). It was observed that secondary cracks branched both perpendicular and parallel from the main fatigue crack at the highest tensile loads and were attributed to excessive strain in the crack vicinity. Formation of secondary cracks during fatigue loading has also been observed for other alloys including, steel (Tang et al. 2019, Smith et al. 1995), aluminium, titanium, and nickel alloys (Gauthier et al. 1973) and was reported to be more prevalent at higher loads (Smith et al. 1995).

Overall, there is a substantial mass of observations of secondary cracks in connection with fatigue pre-cracking, both from the literature and from inspection of the new WOL specimens discussed herein. Based on this evidence the fatigue hypothesis appears to be the most feasible explanation for the formation of the secondary cracks observed on the WOL specimens taken from the MiniCan experiment, which is consistent with the conclusions presented in Smart et al. (2013) and Gordon et al. (2017).

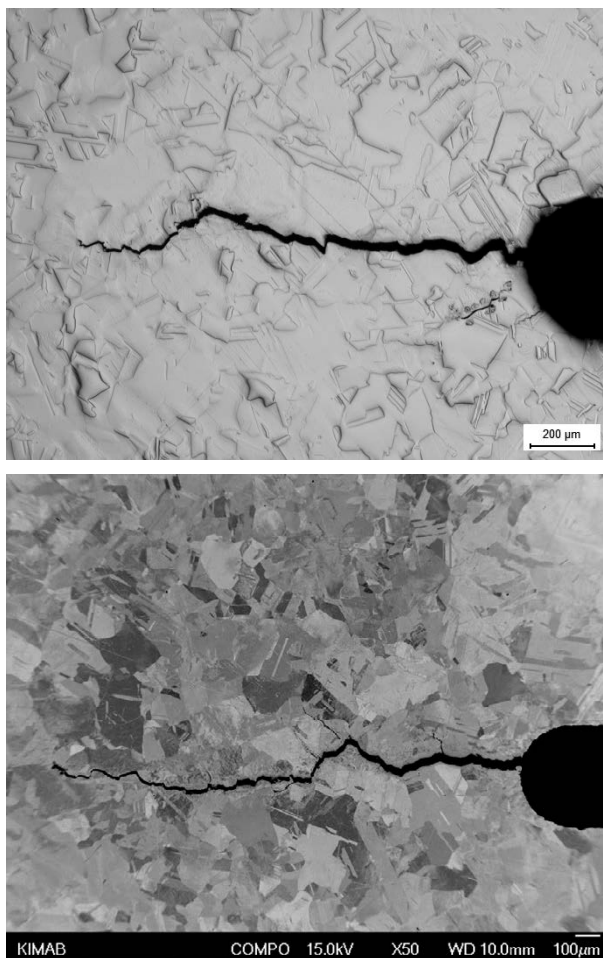


Figure 4-2. Optical (top) and SEM (bottom) micrographs of pre-cracks in WOL specimen M4 3:1, from MiniCan 4 (Figures A3-34 and A3-40 in Gordon et al. (2017).

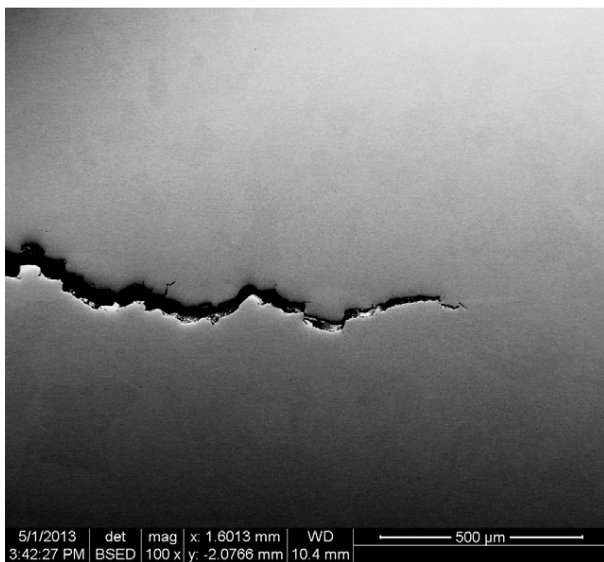
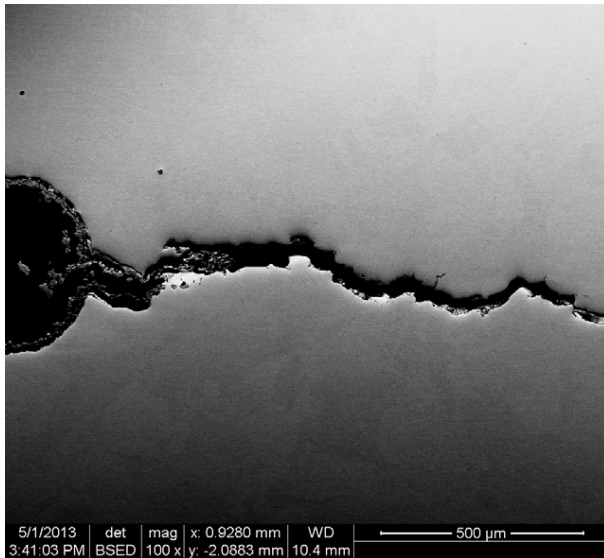


Figure 4-3. SEM micrographs of the pre-crack in WOL specimen 2 from MiniCan 3 (located near to support cage) at the notch (top) and the crack tip (bottom) (Figure 3-27 in Smart et al. (2013)).

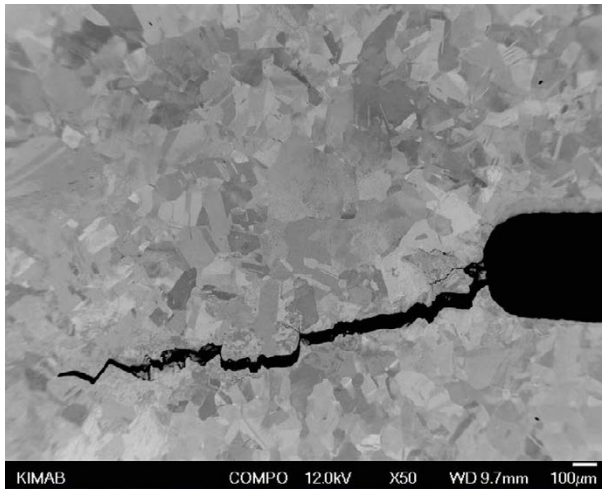


Figure 4-4. SEM backscattered electron micrograph of the pre-crack in WOL specimen M4 4:1 from MiniCan 4 showing the pre-crack emanating from the notch (Figure A3-60 in Gordon et al. (2017)).

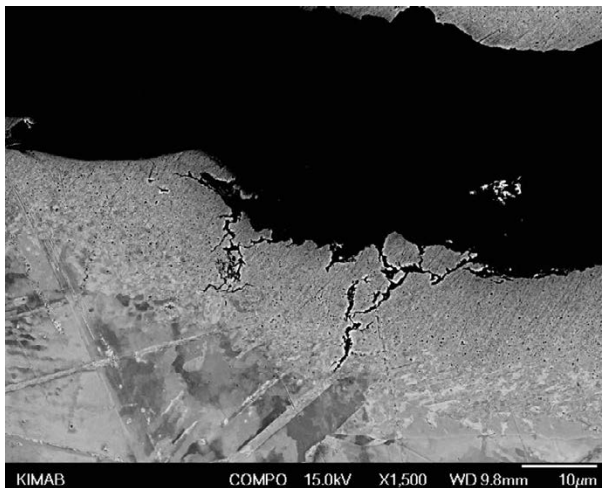


Figure 4-5. SEM image showing detail of the pre-crack of WOL specimen M4 3:1, from MiniCan 4, showing smaller secondary cracks in the cold deformed area of the material (Figure A3-44 in Gordon et al. (2017)).

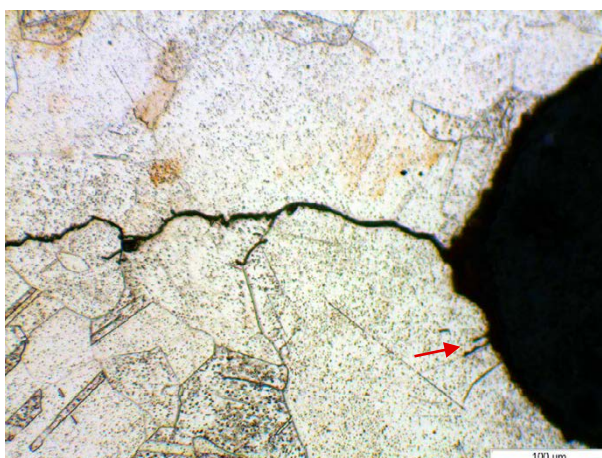


Figure 4-6. Optical image of the pre-crack in WOL specimen 1 from MiniCan 3. Note the ca 40 µm fracture emanating from the notch (red arrow) near the opening of the pre-crack. (Figure 3-18 in Smart et al. (2013)).

5 Conclusions

In this study newly prepared WOL specimens replicating those previously manufactured for the MiniCan experiment (and subsequently exposed to borehole groundwater in that experiment) were examined metallographically. This was done to ascertain whether the procedure used to generate the pre-crack in the specimens also generated secondary cracking, which could otherwise possibly be attributed to SCC during exposure to groundwater. The following conclusions were reached in this study:

- Fatigue pre-cracking of WOL specimens produced cracks with a morphology that closely resembled those observed on unloaded, pre-cracked WOL specimens following exposure to sulphidic groundwater in a borehole for between 4 and 9 years during the MiniCan experiment.
- Cracks that were produced by fatigue only, i.e. with no exposure to the borehole environment, exhibited secondary cracks branching from the main pre-crack, with some secondary cracks orientated perpendicular to it. Multiple crack initiation was also observed from the notch of WOL specimens.
- The presence of secondary cracks and multiple crack initiation from the notch that was observed on unloaded WOL specimens taken from the MiniCan experiment is attributed to the initial fatigue pre-cracking and not stress corrosion cracking during exposure to corrosive groundwater. This conclusion is based on the close resemblance that these crack features have with those that were produced by fatigue only, i.e. with no exposure to the borehole environment.
- The formation of secondary fractures during fatigue loading was further supported by the presence of cracks that emanated perpendicular from the fracture face of the fast fracture region that was formed when fatigue cycling was applied during post-test examination of a WOL specimen from MiniCan 3, in order to open the specimen for inspection of the corroded fracture surface.

References

SKB's (Svensk Kärnbränslehantering AB) publications can be found at www.skb.com/publications.

Aggarwal S, Addepalli V, Smart N, 2015. Further metallographic analysis of MiniCan SCC test specimens. SKB R-15-11, Svensk Kärnbränslehantering AB.

Collini L, 2012. Copper Alloys – Early Applications and Current Performance – Enhancing Processes, ISBN 978-953-51-0160-4.

Forsström A, Becker R, Hänninen H, Yagodzinskyy Y, Heikkilä M, 2021. Sulphide-induced stress corrosion cracking and hydrogen absorption of copper in deoxygenated water at 90 °C. *Materials and Corrosion*, 72 (1-2), 317–332.

Gauthier P, De Rabaudy H, Auvinet J, 1973. Secondary cracking process during fatigue crack propagation. *Engineering Fracture Mechanics*, 5 (4), 977–978.

Gordon A, Sjögren L, Taxen C, Johansson A J, 2017. Retrieval and post-test examination of packages 4 and 5 of the MiniCan field experiment. SKB TR-16-12, Svensk Kärnbränslehantering AB.

Ikeda B M, Litke C D, 2007. Stress corrosion cracking of copper in nitrite/chloride mixtures at elevated temperatures. NWMO TR-2007-04, Nuclear Waste Management Organization, Canada.

ISO 7500-1:2018, 2018. Metallic materials -- Calibration and verification of static uniaxial testing machines -- Part 1: Tension/compression testing machines -- Calibration and verification of the force-measuring system.

Smart N, Rance A, 2009. Miniature canister corrosion experiment – results of operations to May 2008. SKB TR-09-20, Svensk Kärnbränslehantering AB.

Smart N, Rance A, Reddy B, Fennell P, Winsley R, 2012. Analysis of SKB MiniCan. Experiment 3. SKB TR-12-09, Svensk Kärnbränslehantering AB.

Smart N, Rose S, Nixon D, Rance A, 2013. Metallographic analysis of SKB MiniCan experiment 3. SKB R-13-35, Svensk Kärnbränslehantering AB.

Smart N, Reddy B, Nixon D, Rance A, Johansson A J, 2015. Miniature Canister (MiniCan) Corrosion experiment. Progress report 5 for 2008–2013. SKB P-14-19, Svensk Kärnbränslehantering AB.

Smith J, Bassim M N, Liu C D, 1995. Effects of fatigue precracking on stretch zone formation. *Engineering Fracture Mechanics*, 52 (3), 401–408.

SSM, 2019. SSM's external experts' reviews of SKB's report on supplementary information on canister integrity issues. Technical Note Report number: 2019:22 ISSN: 2000-0456, Strålsäkerhetsmyndigheten.

Taniguchi N, Kawasaki M, 2008. Influence of sulfide concentration on the corrosion behavior of pure copper in synthetic seawater. *Journal of Nuclear Materials*, 379, 154–161.

Tang Z, Jing H, Xu L, Chi D, Zhao L, Han Y, Xiao B, Zhang Y, Li H, Wu D, 2019. Crack growth behavior, fracture mechanism, and microstructural evolution of G115 steel under creep-fatigue loading conditions. *International Journal of Mechanical Sciences*, 161–162, 105037.

Taxén C, Núñez A M, Lilja C, 2023. Stress corrosion of copper in sulfide solutions: Variations in pH-buffer, strain rate, and temperature. *Materials and Corrosion*, 74, 1632–1644.

Location of U-bend and WOL specimens in MiniCan borehole

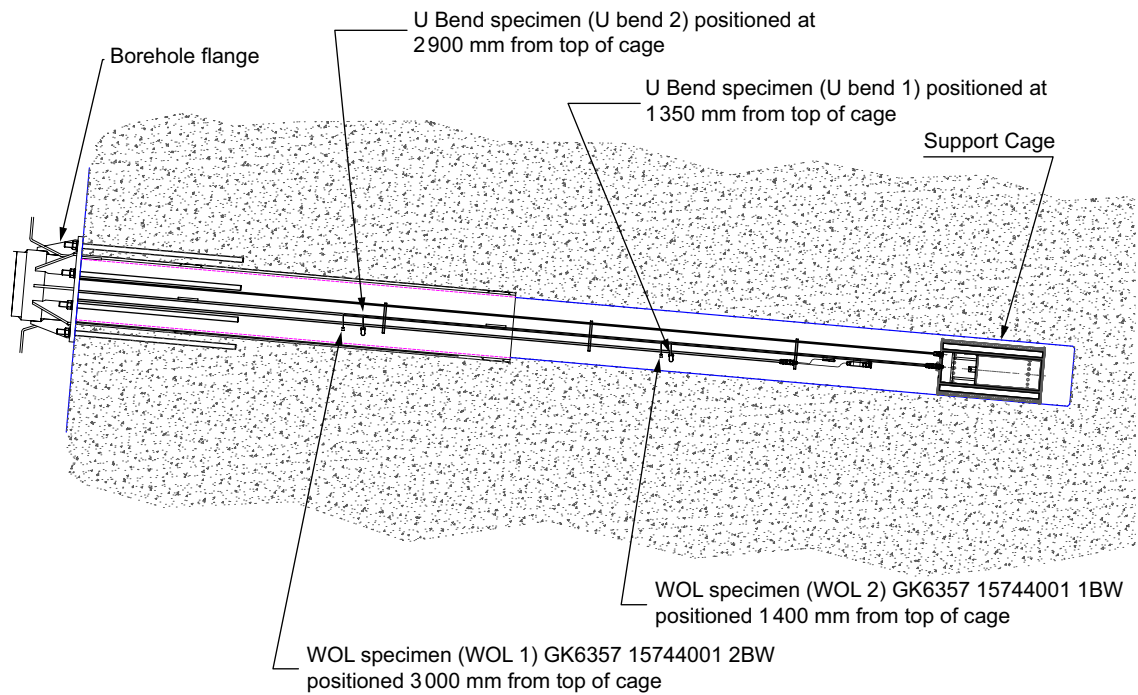


Figure A-1. Location of U-bend and WOL specimens in MiniCan borehole relative to the position of the support cage containing the MiniCan experiment and the borehole flange.

Manufacturing of the original MiniCan WOL specimens

The original fatigue pre-cracking procedure of WOL specimens consisted of the formation of a crack nominally 1.5 mm in length, leading to a crack length-to-width ratio of $a/W \approx 0.4$. The stress intensity factor used was $K_{max} = 8.5 \text{ MPa}\sqrt{\text{m}}$ throughout, with an R-ratio of 0.1. Typically, 550 000 cycles were required to generate the fatigue crack, at a frequency of around 100 Hz. Details of the procedure are shown in Figure B-1. After exposure in the borehole, specimens were sectioned for analysis as shown in Figure B-2.

A diagram of the WOL specimen design that was used in the MiniCan experiment and subsequently for the new WOL specimens is shown in Figure B-3.

Structural Integrity Services Department - Materials Testing Laboratory

CT PRECRACKING CALCULATION SHEET	MTL Job No. 6357	Issue No. 9								
SPREADSHEET NAME: PC CT		VERSION No. 2								
DESCRIPTION Spreadsheet for calculating precracking loads. Specimen type: CT only. Room temp. pre-cracking only. Calculation basis: From $K=(PY)/(BW^{0.5})$ using a/W at the end of the step										
INSTRUCTIONS Enter the data required in the BOLD outline boxes (pink on screen). Print out the table & sign.										
SPECIMEN DETAILS	MATERIAL DETAILS									
Thickness, B, mm 6.25	Yield/proof stress, MPa 75									
Width, W, mm 12	Tensile strength, MPa 150									
Machined notch length, mm 3.3	Elastic modulus, GPa 117									
	Estimated KIC, $\text{MPa}\sqrt{\text{m}}$ 50									
CRACK REQUIREMENTS	K REQUIREMENTS									
Required a/W 0.4	Start K, $\text{MPa}\sqrt{\text{m}}$ 8.5									
Number of steps 3	End K, $\text{MPa}\sqrt{\text{m}}$ 8.5									
Length of last step, mm* 0	R ratio 0.1									
CALCULATED VALUES										
Length of crack, mm 1.5	Final crack length, mm 4.8									
LOAD TABLE										
Step No.	Crack length, mm		P/c mm	a/W	Kmax $\text{MPa}\sqrt{\text{m}}$	Pmax kN	Pmin kN	Pmean kN	ΔP \pm kN	BFM** mm
	Start	End								
1	3.300	3.800	0.500	0.317	8.5	0.99	0.10	0.55	0.45	8.200
2	3.800	4.300	1.000	0.358	8.5	0.89	0.09	0.49	0.40	7.700
3	4.300	4.800	1.500	0.400	8.5	0.80	0.08	0.44	0.36	7.200
VALIDITY See Tables on Page 2										
Number of validity failures reported is 5	Number of warnings activated is 2									
COMMENTS										
SIGNED (Test officer)	CHECKED/ APPROVED									

Figure B-1. Parameters for pre-cracking.

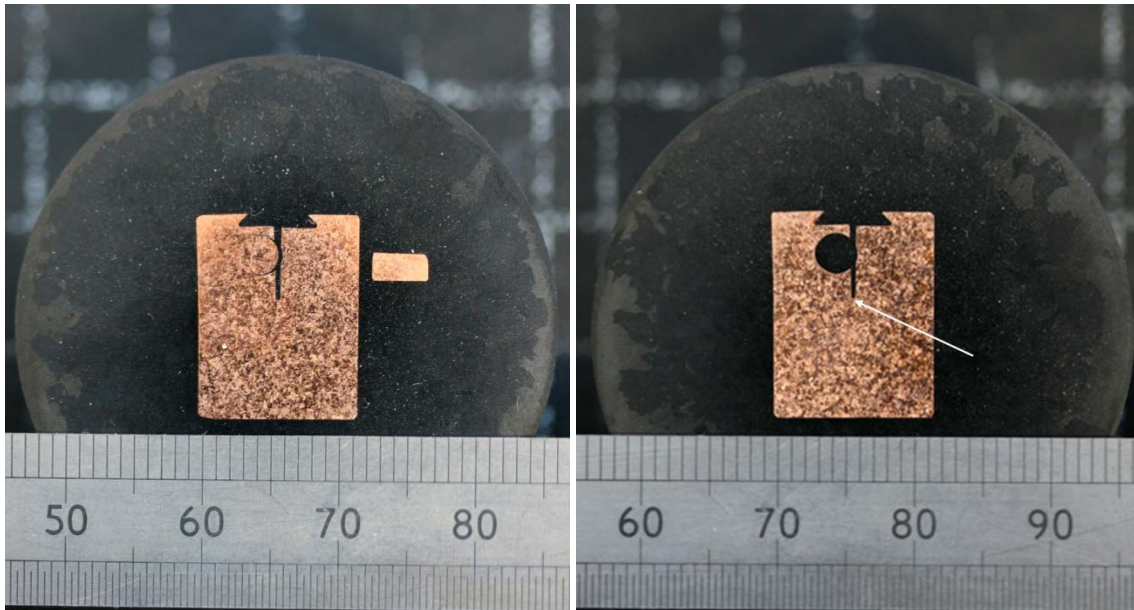


Figure B-2. Sectioning of WOL specimens from the MiniCan experiment. The arrow in the right photograph indicates the location of the notch from which the pre-crack initiates. The direction of the pre-crack is a continuation of the notch.

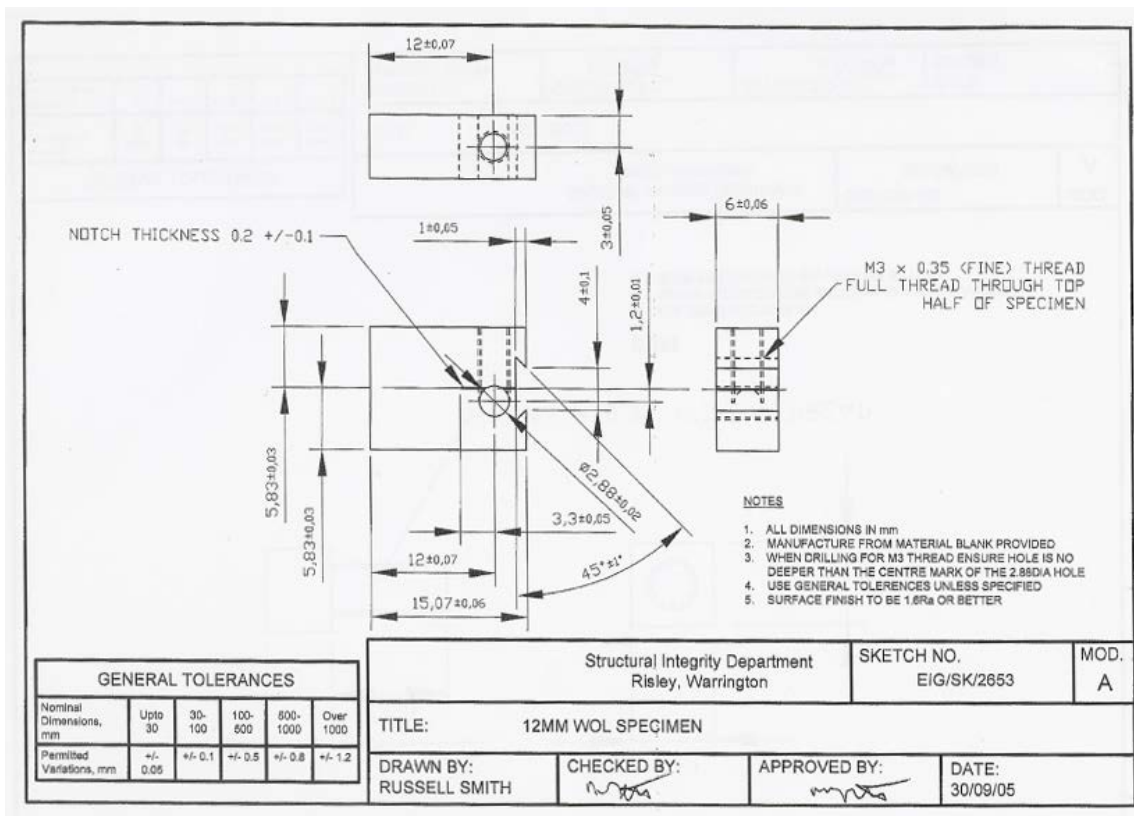


Figure B-3. Original drawing of WOL specimens from the MiniCan experiment.

Preparation of new WOL specimens

During initial attempts to perform fatigue pre-cracking of the specimens the specimens were overloaded, leading to plastic deformation prior to the formation of a crack. Images of an overloaded WOL specimens are shown in Figure C-1 to C-2.



Figure C-1. Side view of overloaded WOL specimen.



Figure C-2. Top view of overloaded WOL specimen.

Several engineers, including external calibration contractors, examined the rig in an attempt to determine what was causing the overload. Initially, the rig's calibration was checked and was found in date. Whilst waiting for further specimens to be prepared, the machine was re-purposed for other specimens. When loading these other specimens (25 mm compact tension specimens) overload was not observed. However, when small, three-point bend specimens were attempted to be pre-cracked, overload was also observed. It was postulated that, when the rig was energised, this caused a jump in the rig's magnetic control, due to the machine's age. It was believed that, due to the specimens' small size, this initial jump was enough to cause an overload. To avoid the potential jump when energising the rig, the rig was subsequently energised without a specimen, then the specimen was inserted. However, when an initial static load was applied, this specimen also became overloaded. Lastly, the rig was completely stripped down, examined and re-assembled. The rig was then recalibrated, which passed with the same values as the previous calibration. A new specimen was then installed into rig and the static load applied. The specimen appeared to remain intact, so the oscillating load was gradually applied. This too did not overload the specimen. The specimen then underwent the same load conditions as the original specimens and was run to the required crack length.

